Physics of negative ions and helicon waves in a resonant antenna plasma source for neutral beams

I. Furno, R. Agnello, Ph. Guittienne, A.A. Howling, R. Jacquier, G. Plyushchev, C. Stollberg, S. Bechu[1], M. Barbisan[2], M. Fadone[2], R. Paqualotto[2], A. Simonin[3]

Ecole Polytechnique Fédérale de Lausanne (EPFL), Swiss Plasma Center (SPC), CH-1015 Lausanne, Switzerland,
[1]Laboratoire de Physique Subatomique et de Cosmologie, Université Grenoble-Alpes, CNRS/IN2P3, Grenoble F-38026, France
[2]Consorzio RFX, Corso Stati Uniti 4, I-35127, Padova, Italy
[3]CEA, IRFM, F-13108, St-Paul-lez-Durance, France

1. In short

- **Helicon sources for NBIs**
  - Helicon plasmas as negative ion sources could have advantages over traditional ICPs:
    - 1) reduced RF power
    - 2) stable operation at low pressure (< 0.3 Pa) resulting in low electron stripping losses
    - 3) higher efficiency of negative ion production in volume production mode, and a high degree of molecular dissociation, which would be favorable in a caesiated source
    - 4) by producing a magnetized plasma column, they are well-adapted to a blade-shape geometry, such as those required for photo-neutralizer-based NBIs
- **RAID [1] is a high-power (up to 20kW) helicon source equipped with resonant antennas [2]**
  - Helicon plasmas in hydrogen and deuterium can be produced and sustained in steady-state
  - RAID plasmas exhibit a negative ion-rich shell
  - The maximum negative ion density increases with injected RF power
- **A 1.5 D fluid model coupled to experimental T_e and n_e profiles reproduces many observed features**
  - Negative ions are generated by dissociative attachment on ro-vibrationally excited H_2 molecules
  - In the plasma column center, hot electrons destroy H^- by electron detachment and mutual neutralization. At the edge of the plasma column, atomic detachment destroys H^-
- **Extraction of negative ions**
  - A radial extractor has been developed
  - First experiments demonstrated negative ion extraction

2. The Resonant Antenna Ion Device (RAID) [1]

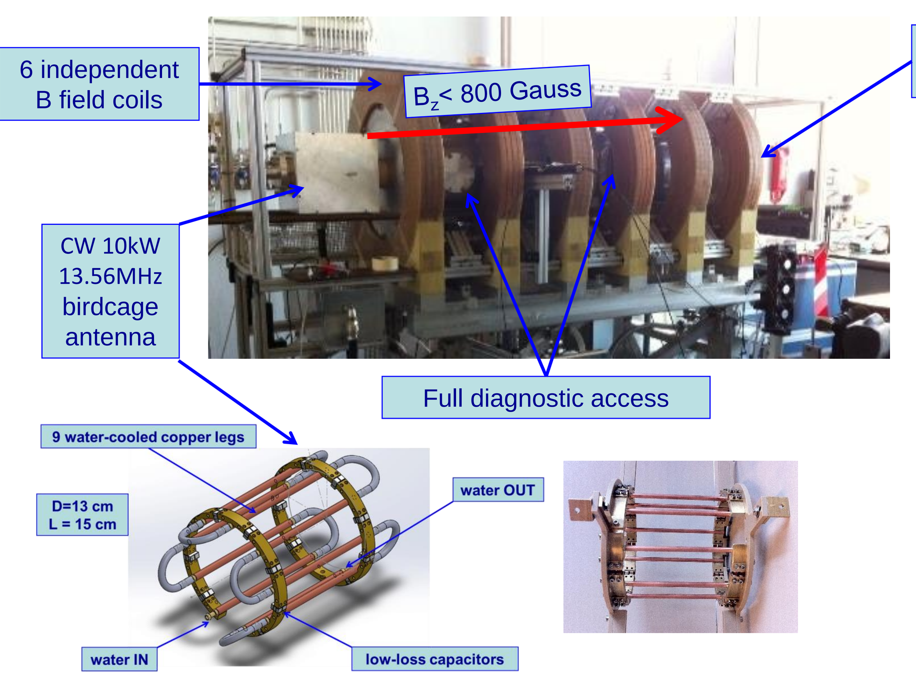

- **Diagnostics**
  - **Langmuir probes [7, 8]**
  - **B-dot (magnetic) probes [3]**
  - **Microwave interferometer [9]**
  - **Thomson scattering system [10]**
  - **Cavity Ring Down Spectroscopy [11]**
  - **LP-laser photodetachment [11]**
  - **Optical emission Spectroscopy [12]**

FIG 1 : Left - The Resonant Antenna Ion device (RAID) with a few ancillaries.

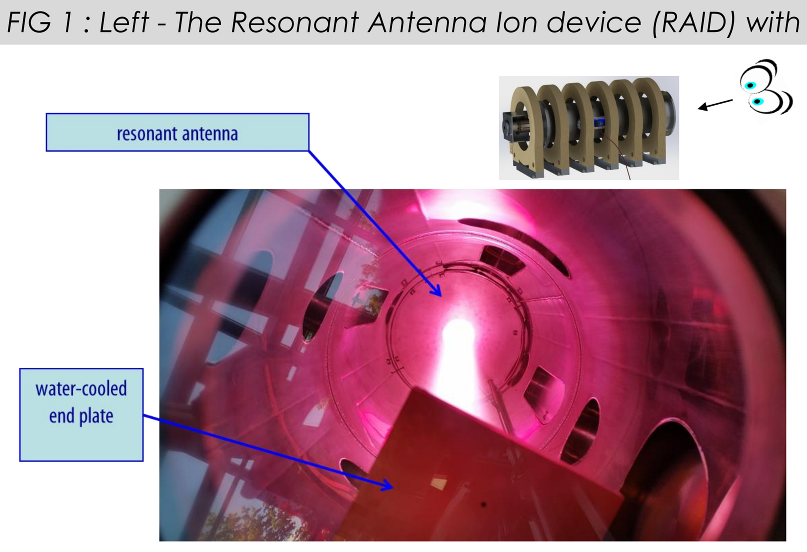

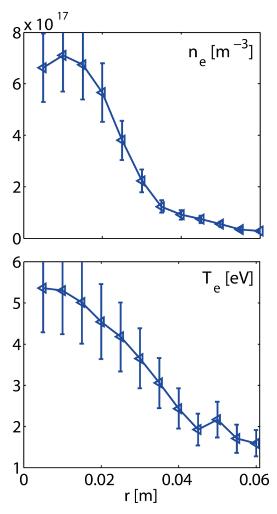

Parameter	Value
Gas pressure	0.1 - 1.5 Pa
Magnetic field	0.01 - 0.08 T
Plasma Density	$10^{16} - 5\times10^{18}$ m^{-3}
Electron Temperature	1 - 8 eV
Ion temperature	0.08 - 0.12 eV
Ion cyclotron frequency	~ 300 kHz (B = 20 mT)
Electron cyclotron frequency	~ 560 MHz
Ion-H_2 collision frequency	~ 4 kHz
Neutral mean free path	~ 0.1 m
Ion Larmor radius	r_L 1 mm
Electron Larmor Radius	r_L 0.25 mm

TABLE I: Typical parameters for a hydrogen plasma discharge in RAID.

FIG 2 : Left – Visible light from the RAID plasma column. Right Typical T_e and n_e profiles (50 cm away from the antenna)

3. Physics of helicon waves [3 ,4]

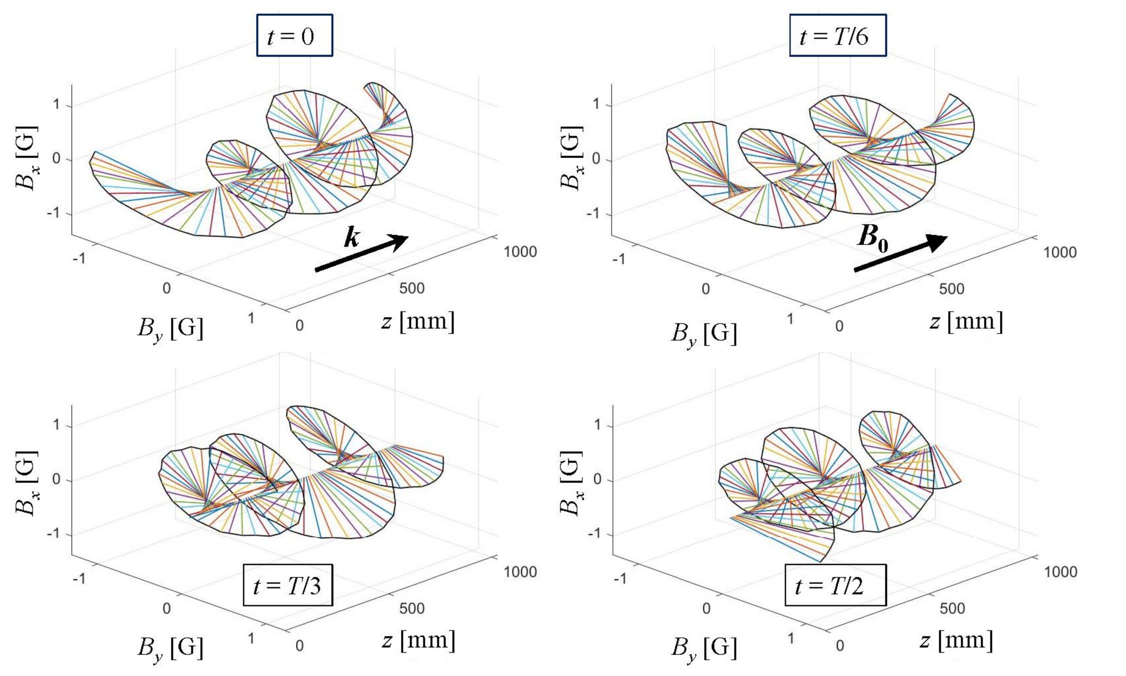

FIG 2: The transverse magnetic field raw data, measured on axis, for three equal time intervals during a RF half-period (t = 0; T/6; T/3; T/2). The static magnetic field B_0, and the wave vector k of propagation, are both oriented along the +z axis as shown in the figure. Each chord is a perpendicular from the plasma column axis, at the z position where the measurement was made, to the $[B_x, B_y]$ value measured at that position. The helix is the locus of these $[B_x, B_y, z]$ points. The magnetic field spatial structure is seen to be a left-handed helix, rotating clockwise with respect to the direction of B_0, in agreement with helicon theory. Hydrogen at 0.3 Pa, B_0 = 200 G, PRF = 1.5 kW.

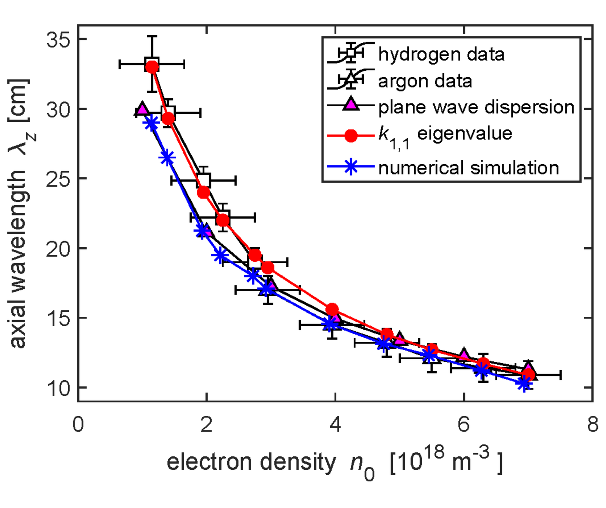

FIG. 3: Variation of the axial wavelength as a function of the peak electron density n_0 for B_0 = 200 G, showing a comparison between experimental data, analytical, and numerical results. The open symbols (partly obscured) represent the experimentally measured axial wavelengths. The magenta triangles indicate the plane wave dispersion relation for an assumed average density n_e = $0.5n_0$. The full red circles correspond to the k_{11}. The blue stars show the results of the COMSOL numerical simulations. Details can be found in Ref. [4].

4. The physics of negative ions [10, 11, 12]

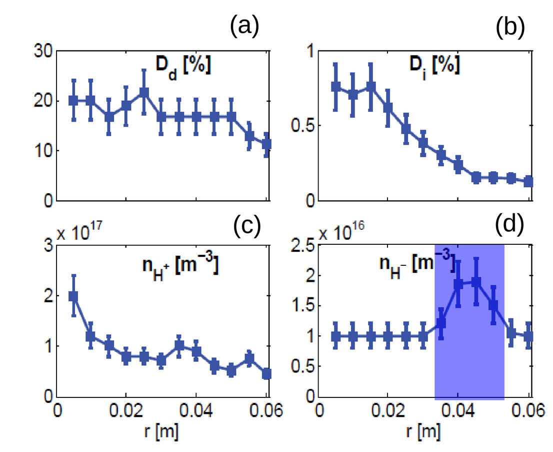

Ratio atomic/molec. density

$$D_d = \frac{f}{f+2}$$

$$D_i = \frac{n_e}{n_H + n_{H_2}}$$

FIG. 5: Early measurements were obtained with OES and revealed highly dissociated plasmas with the presence of a negative ion shell (blue-shaded region in (d)). In the figure we show profiles of (a) degree of dissociation D_d, (b) degree of ionization D_i, (c) H^+ density and (d) H^- density estimated by YACORA [13] for an input power of 3 kW in hydrogen.

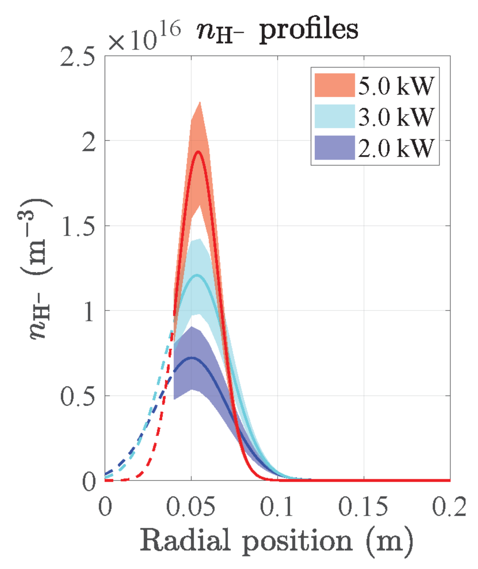

FIG. 6: Radial profiles of negative ions in H_2 plasmas (deuterium not shown) for different powers obtained using the relative negative ion profiles measured with laser photo-detachment and calibrated with CRDS line-integrated measurements. A cyclindrical shell centered at approximately 5.5 cm shows the presence of negative ions with density of the order of 10^{16} m^{-3}.

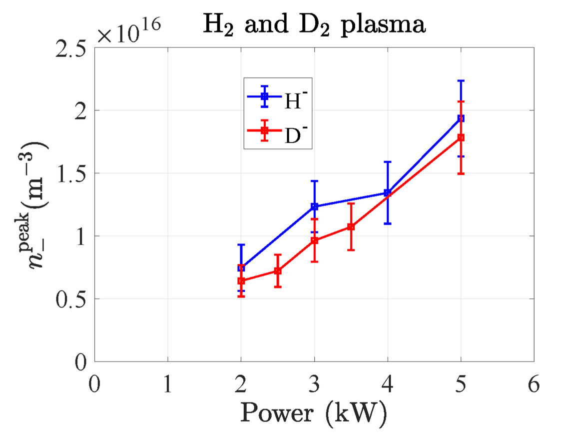

FIG. 7: The scaling of the negative ion density with power

5. 1.5D fluid model and complex H/D chemistry [5, 6, 9]

Ions

Sources Losses

Continuity $\quad \dfrac{\partial n_s}{\partial t} + \nabla\Gamma_s = S_s - L_s \qquad$ s = H^-, H^+, H_2^+, H_3^+

Momentum $\quad m_s n_s\left[\dfrac{\partial \bar{v}_s}{\partial t} + (\bar{v}_s\cdot\nabla)\bar{v}_s\right] = q_s n_s\left(\bar{E} + \bar{v}_s\times\bar{B}\right) - \nabla\bar{\bar{P}} - m_s n_s \upsilon_s \bar{v}_s$

Poisson $\quad \varepsilon_0\nabla^2 V = -\sum_s q_s\left(n_s - n_e\right)$

Electrons $\quad \rightarrow$ Experimental profiles of T_e and n_e

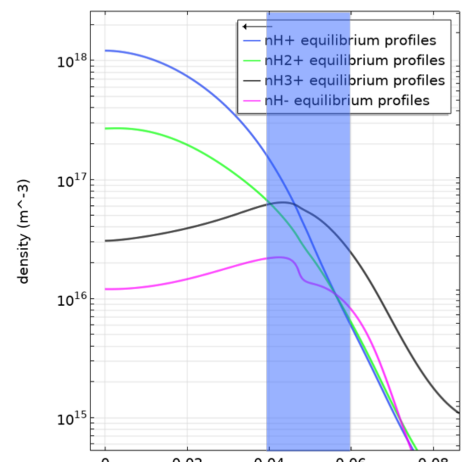

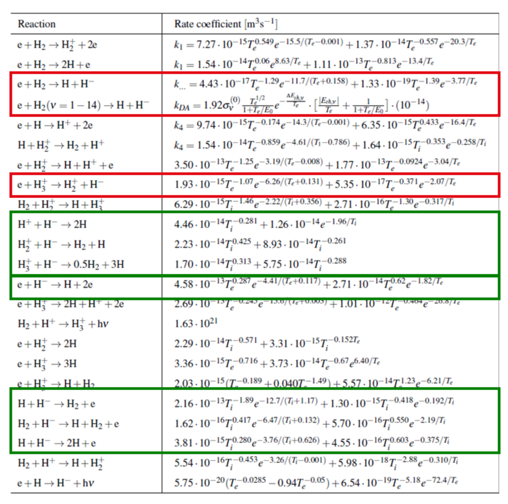

Dissociative Attachment

Ion/pair formation

Mutual Neutralization

Electron Detachment

Atom./Molec. Detachment

Electron Attachment

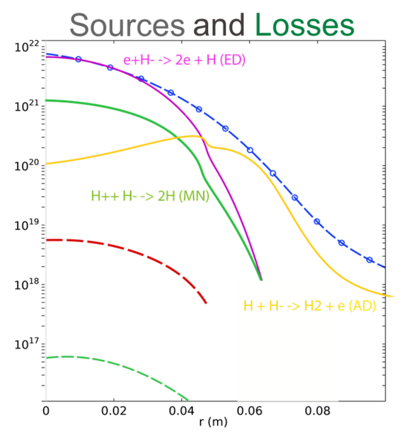

Dissociative attachment to $H_2(v)$ is by far the largest H^- production channel

In the center of the plasma column, hot electrons destroy H^- by electron detachment (ED) and mutual neutralization (MN)

At the edge of the plasma column, atomic detachment (AD) destroys H^-

6. Negative ion extractor design and first experiments

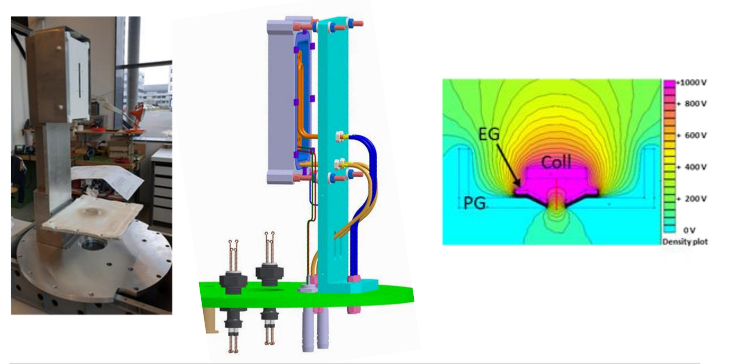

FIG 8: A radial extractor through an axial slit has been designed and manufactured. The radial extractor geometry has the advantage of having an intrinsic magnetic filter field, provided by the RAID background magnetic field B_0. The design of the extractor is performed using FEMM 4.2 [14] and COMSOL [15] and IBSimu [16]. A system with three grids imposes a large electric field in the region of extraction, which efficiently separates the plasma from the beam region. This geometry has also an effect on the electron and negative ion currents, which can be extracted due to the Child-Langmuir limit. Specifically, the Langmuir-Blodgett law is used for the cylindrical case, which is the relevant model for the radial extraction.

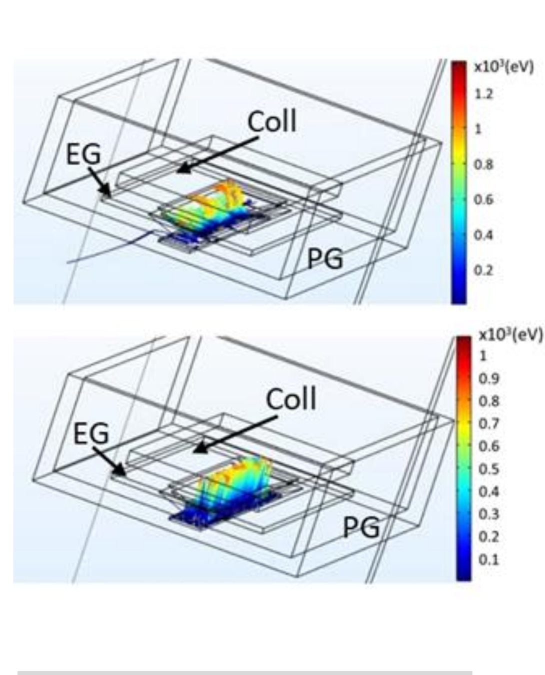

FIG 9: 3D-COMSOL particle simulations showing (top) electron suppression to the extraction grid (EG) and (bottom) negative ion trajectories. All particles hit the collector electrode.

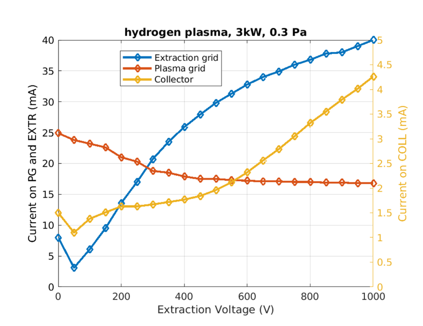

FIG 10: First extraction experiments. The plasma grid is placed at r=6 cm. The extractor, collector and plasma grid currents are measured. The current on the extraction grid is mostly due to electrons transported by E×B drift. The current on the collector is mostly carried by negative ions and shows an almost linear dependence. This indicates that the extractor is here operated below the Child-Langmuir limit.

References

[1] I. Furno et al., EPJ Web of Conferences 157, 03014 (2017).

[2] Ph. Guitttienne et al., J. Appl. Phys. 98, 083304 (2005).

[3] R. Jacquier et al., Fusion Engineering and Design 146, 1140 (2019).

[4] Ph. Guittienne et al., *Helicon wave plasma generated by a resonant birdcage antenna: Magnetic field measurements and analysis in the RAID linear device*, submitted to Plasma Sci. Sour. Tech.

[5] R. Agnello et al., *1.5D fluid model of a hydrogen helicon plasma discharge*, in preparation.

[6] G. Fubiani et al., *Negative hydrogen ion dynamics inside the plasma volume of a linear device: estimates from Particle-In-Cell calculations*, submitted to Phys. Plasmas.

[7] Ph. Guittienne et al., Phys. Plasmas 25, 093519 (2018).

[8] A. A. Howling et al., Phys. Plasmas 26, 044502 (2019).

[9] R. Agnello, *Negative Hydrogen Ions in a Helicon Plasma Source*, EPFL Thesis 7817 (2020).

[10] R. Agnello et al., J. Plasma Phys. 86, 905860306 (2020).

[11] R. Agnello et al., Rev. Sci. Instrum. 89, 103504 (2018); R. Agnello et al., Nucl. Fusion 60, 026007 (2019)

[12] C. Marini et al., Nucl. Fusion 57, 036024 (2017).

[13] D. Wunderlich, S. Dietrich and U. Fantz, J. Quant. Spectrosc. Radiat. Transfer 110, 62 (2009).

[14] https://www.femm.info/wiki/HomePage

[15] COMSOL Multiphysics® v. 5.4. www.comsol.com. COMSOL AB, Stockholm, Sweden.

[16] http://ibsimu.sourceforge.net/

This work was supported in part by the Swiss National Science Foundation

EUROfusion

This work has been carried out within the framework of the EUROfusion Consortium and has received funding from the Euratom research and training programme 2014-2018 and 2019-2020 under grant agreement No 633053.
The views and opinions expressed herein do not necessarily reflect those of the European Commission.